Hybrid Modeling Based Co-optimization of Crew Dispatch and Distribution System Restoration Considering Multiple Uncertainties

Jiayong Li, *Member, IEEE*, Mohammad E. Khodayar, *Senior Member, IEEE*, Mohammad Ramin Feizi, *Student Member, IEEE*

***Abstract*—Natural disasters could lead to large-scale power outages by causing severe damages to distribution networks (DNs). Developing highly efficient outage management schemes is imperative for expediting service restoration. To this end, a novel multi-stage co-optimization model is proposed to seamlessly integrate the repair crew dispatch with the distribution system restoration. Furthermore, multiple sources of uncertainties are incorporated. To properly handle these uncertainties, a novel hybrid modeling approach is developed. In particular, the first stage is cast as a deterministic optimization problem to determine the crew route option prior to the realization of uncertainties. The second stage is to reconfigure the DN for forming multi-microgrids considering the uncertainties in crew travel time and repair time, which is formulated as a stochastic program. In the third stage, a robust optimization framework is applied to acquire a scheduling plan of various distributed energy resources that is immune to the worst-case realizations of electricity demand and PV generation. Finally, an advanced solution method is devised to achieve the computational tractability based on constraint and column generation and progressive hedging approaches. Numerical tests on the modified IEEE 37-bus DN show that the computation performance of the proposed solution method well fits the real-time application and also demonstrate that the highest demand curtailment is reduced by 3.3% and the variance of the restoration outcome is lowered by 40.5% compared with a recently proposed benchmark.**

***Index Terms*—Repair crew dispatch, distribution system restoration, uncertainties, hybrid modeling, demand curtailment.**

NOMENCLATURE

Indices and sets:

$\mathcal{D}^R$	Set of repair crew depot sites
$\mathcal{F}^R$	Set of damaged component sites
$s/\mathcal{S}$	Index/set of scenarios
$t/\mathcal{T}$	Index/set of time intervals
$k/\mathcal{K}$	Index/set of bus blocks
$\mathcal{L}/\mathcal{N}$	Set of lines/buses
$\mathcal{N}^{dg}/\mathcal{N}^{pv}/\mathcal{N}^{es}$	Set of buses with DG/PV/ESS installations

Parameters:

$p_{i,t}^{dn}/p_{i,t}^{pvn}$	Nominal load demand/PV output at bus i at time t
$\hat{p}_{i,t}^{d}/\hat{p}_{i,t}^{pv}$	Maximum deviation of load demand/PV output from the nominal value at bus i at time t
Γ_N^d/Γ_T^d	Spatial/temporal uncertainty budget for load demand
$\Gamma_N^{pv}/\Gamma_T^{pv}$	Spatial/temporal uncertainty budget for PV output
N_i^R	Total number of crews stationed in depot i
$T_{ij,s}$	Travel time from site i to site j in scenario s
$T_{i,s}^R$	Repair time for damaged component i in scenario s
$\Pr(s)$	Probability of scenario s
c_t^{grid}	Energy purchasing price from main grid at time t
c_i^{dg}	Unit generation cost of DG unit i
$c_{i,t}^{d}$	Unit cost for load curtailment at bus i at time t
r_{ij}/x_{ij}	Resistance/reactance of line (i,j)
$\underline{p}_i^{dg}/\overline{p}_i^{dg}$	The lower/upper limit of the active power of DG i
$\underline{q}_i^{dg}/\overline{q}_i^{dg}$	The lower/upper limit of the reactive power of DG i
S_i^{pv}	Rated apparent power capacity of PV unit i
$\overline{p}_i^{ch}/\overline{p}_i^{dch}$	Maximum allowed charging/discharging power of ESS i
η_i^{ch}/η_i^{dch}	Charging/discharging efficiency of ESS i
$\overline{\text{SoC}}_i/\underline{\text{SoC}}_i$	Maximum/minimum allowed SOC of ESS i

Variables:

$z_{i,t}^{du}/z_{i,t}^{dl}$	Binary variable indicating whether load i attains the upper/lower bound
$z_{i,t}^{pvu}/z_{i,t}^{pvl}$	Binary variable indicating whether the active power output of PV i attains the upper/lower bound
x_{ij}^R	Binary entry of the route table
$T_{i,s}^A$	Repair crew arrival time at site i in scenario s
$e_{i,t,s}$	Binary variable indicating whether the repair completion time of damage i is within time interval t
$u_{jk,t,s}$	Binary variable indicating the availability of line (j,k) at time t in scenario s
$y_{k,t,s}$	Binary variable indicating the energization status of bus block k at time t in scenario s

Jiayong Li is with the College of Electrical and Information Engineering, Hunan University, Changsha 410082, China, and also with the Department of Electrical and Computer Engineering, Southern Methodist University, Dallas, TX 75275 USA (emails: j-y.li@connect.polyu.hk).

Mohammad E. Khodayar and Mohammad R. Feizi are with the Department of Electrical and Computer Engineering, Southern Methodist University, Dallas, TX 75275 USA (emails: mkhodayar@smu.edu, mfeizi@smu.edu).

This work is supported in part by the U.S. Department of Energys Solar Energy Technologies Office under Grant CPS34228, in part by the National Science Foundation under Grant ECCS-1710923, and in part by the National Natural Science Foundation of China under Grant 51907056.

$g_{i,t,s}$ Virtual generation of DG i at time t

$f_{ik,t,s}$ Virtual power flow on line (i,k) at time t

$z^{es}_{i,t,s}$ Binary variable indicating the actual charging status of ESS i at time t

$P_{ij,t,s}/Q_{ij,t,s}$ Active/reactive power flows on line (i,j)

$v_{i,t,s}$ Squared nodal voltage magnitude of bus i at time t

$p^{d}_{i,t,s}/q^{d}_{i,t,s}$ Served active/reactive load at bus i at time t

$\overline{p}^{d}_{i,t}$ Uncertain total active load at bus i at time t

$p^{dg}_{i,t,s}/q^{dg}_{i,t,s}$ Active/reactive power output of DG i at time t

$p^{pv}_{i,t,s}/q^{pv}_{i,t,s}$ Active/reactive power output of PV i at time t

$p^{ch}_{i,t,s}/p^{dch}_{i,t,s}$ Charging/discharging power of ESS i at time t

$\mathrm{SoC}_{i,t,s}$ State of charge of ESS i at time t

$\overline{p}^{pv}_{i,t}$ Uncertain maximum available active power output of PV i at time t

$\mathbf{x}$ Vector of first-stage decision variables

$\mathbf{y}_s/\mathbf{z}_s$ Vector of second-stage/third-stage variables for scenario s

$\mathbf{u}_s$ Vector of the third-stage uncertainty variables for scenario s

I. Introduction

NATURAL disasters, such as storms and floods, can cause severe damages to the power distribution infrastructures which could further lead to large-scale blackouts [1]. Extensive power outages have been experienced recently due to the destructions caused by hurricanes Nate, Maria, Irma, and Harvey [2]. Such power outages could impede the post-disaster recovery and life-line rescue by affecting the normal operations of other dependent infrastructure systems [3]. Although the topic of power distribution resilience has been widely investigated, most works merely focused on the distribution system restoration (DSR) task alone and overlooked the interdependence between the repair scheduling and DSR. Hence, there is an urgent need for an efficient outage management scheme that is able to seamlessly integrate the repair scheduling with the DSR to expedite service restoration.

The DSR procedure is generally performed through network reconfigurations [4]. To name a few, in [5], a distribution system (DS) reconfiguration strategy was proposed to redistribute loads among feeders for service restoration. Ref. [6] presented a self-healing scheme for DSs using a two-stage network reconfiguration method. In [7], a multi-agent system based network reconfiguration approach was developed to reduce the computational dimensions of service restoration. In [8], a new formulation of radiality constraints was presented so as to have extended flexibility of DS reconfiguration.

Recently, the fast developments in distributed energy resources (DERs), demand response (DR), and microgrids are transforming the operation and control paradigms of DS [9] and thus facilitate the design of advanced DSR schemes to fully leverage the advantages of DERs. For instance, ref. [10] developed a network reconfiguration strategy in presence of distributed energy storage to minimize the cost of service restoration. In [11], the benefits of DR were verified for improving the resilience of dynamically-clustered microgrids. In [12], distributed generators (DGs) were deployed to accelerate DSR and the DG start-up sequences were considered to reduce the number of switching operations. In [13], the restoration capability of DSs was enhanced by combining the reconfiguration and application of microgrids. In [14], the networked multi-microgrids were investigated to minimize the unserved critical loads after power outages.

Since DS cannot be fully restored before the clearance of damages, researches on repair scheduling (RS) have also been conducted to reduce the adverse effects of power outages [15]. For example, in [16], a post-hurricane recovery model was proposed to mobilize the repair crews among different damaged sites. In [17], a strategical RS approach was presented by formulating the problem as a time-indexed integer linear program. In [18], the authors investigated the coordinated repair crew dispatch for the interdependent electricity and natural gas networks. Nevertheless, all aforementioned researches either only focused on DSR or on the repair scheduling, and overlooked the interdependence between these two tasks.

To resolve this issue, a few efforts [19]–[21] have been made towards coordination of RS and DSR. Ref. [19] proposed a synthetic model to implement multiple tasks in DSR in a coordinated manner by capturing the interdependence between crew dispatch and switching operations. In [21], a disaster recovery logistic model that co-optimized the repair crew and mobile power sources dispatches, was formulated. Nonetheless, the issue of coordination between repair crew dispatch and sequential DSR process has not been well addressed as these models failed to account for the dynamical variations of system operating conditions. Furthermore, these works also did not consider various uncertainties in repair scheduling, electricity demand, and renewable energy generation which could dramatically impact the restoration process.

Stochastic programming (SP) and robust optimization (RO) are two common approaches used for handling the uncertainties in power system operation [22], [23]. In [22], a stochastic framework was presented for the DSR problem considering the uncertainties associated with the power received from the transmission network. Basically, SP relies on the probability distribution functions (PDFs) of the random variables for the generation of scenarios to procure the solution [24]. However, acquiring the accurate PDFs for some random variables, especially the time-varying random variables such as demand and photovoltaic (PV) generation, is a challenging task. In contrast, RO only requires a limited amount of information about the uncertainties and is more computationally tractable. In [23], a robust restoration model was presented where the DG outputs and demands are represented by adjustable uncertainty set.

To sum up, most existing works failed to account for the interdependence between repair scheduling and DSR. Moreover, previous works also failed to incorporate multiple sources of uncertainties including the uncertainties in travel time, repair time, electricity demand and renewable power generation. To bridge these gaps, this paper proposes an advanced outage management scheme to co-optimize repair crew dispatch and DSR taking multiple sources of uncertainties into account. The contributions of this paper are three-fold:

- Unlike the most exiting works that merely focused on a single task, i.e. either repair scheduling or DSR, a novel multi-stage integrated model is proposed in this paper for the co-optimization of crew dispatch and DSR. In particular, a route table is introduced to link the crew dispatch decision with the post-event DS reconfiguration which is further integrated with the microgrid dispatch.
- Multiple sources of uncertainties are incorporated in the proposed model. To properly handle these uncertainties, an innovative hybrid modeling approach is developed. Specifically, the first stage is cast as a deterministic problem for the determination of crew route option. The second and third stages are formulated as a SP problem and a RO problem, respectively. Consequently, both the benefits of SP and RO can be achieved simultaneously.
- To make the proposed model computationally tractable, an efficient solution method is developed based on the constraint and column generation (CCG) and progressive hedging (PH) approaches. Numerical test verifies that the computation performance of the proposed method well fits the real-time application.

The remainder of this paper is organized as follows. Section II presents the problem formulation of the multi-stage co-optimization problem with multiple sources of uncertainties. In Section III, an efficient solution method is presented for solving the proposed model. Section IV demonstrates the numerical results on the modified IEEE 37-bus DS. Finally, Section V concludes this paper.

II. Problem Formulation

A. Framework of the Multi-stage Co-optimization Model

The outage management consists of four steps, namely, information collection, fault positioning and assessment, crew dispatch and distribution system restoration [25]. This paper mainly focuses on the last two phases and assumes that the previous two have been performed. Since the decisions in outage management are implemented sequentially, the co-optimization of crew dispatch and distribution system restoration is modeled as a multi-stage problem whose framework is illustrated in Fig. 1. As shown in the figure, the first stage is to determine the repair crew route solution prior to the realization of the uncertainties in the following two stages. Then, in the second stage, the repair completion times of damages are derived by combining the crew route decision with the crew travel time and the repair time for each damaged component. Consequently, the line availability status at each time interval can be acquired to carry out the network reconfiguration through the sequential switching operation. In the third stage, the scheduling of DERs as well as the demand curtailment will be determined for the previously formed multi-microgrids that incorporate the uncertainties of the maximum available PV output and electricity demand. The overall objective is to minimize the system operation cost plus the demand curtailment cost. Note that there are two categories of uncertainties in the multi-stage co-optimization problem. The first category captures the crew travel time and the repair times of individual damages, which emerges in the second stage and is represented by a set of scenarios. The estimation of these variables is relatively reliable owing to the effective information collection and fault assessment. The second category of uncertainties is associated with the maximum available PV power and the electricity demand. Such resources are represented by an uncertainty set as the predication of these resources is a challenging task. Moreover, the accurate PDFs of PV power and electricity demand are practically unavailable. Therefore, the second stage is modeled as a stochastic programming, while the third stage is formulated as a RO problem.

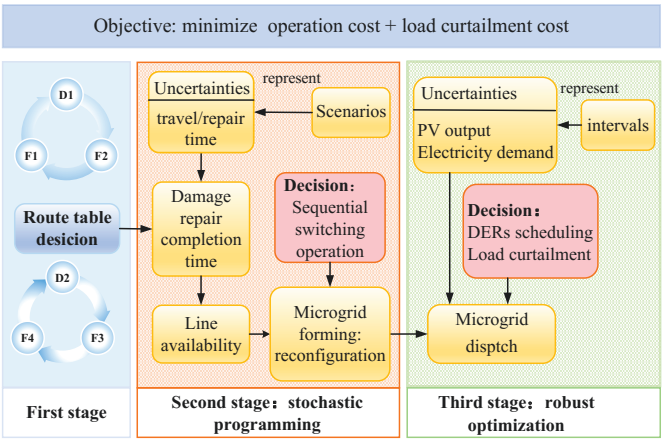

Fig. 1. Framework for the hybrid modeling of the proposed multi-stage co-optimization problem

B. Multiple Sources of Uncertainties

As recommended by [26], the uncertainties in repair time and travel time are represented by the truncated lognormal distribution and truncated normal distribution, respectively. A finite number of scenarios including the travel time and repair time are generated using the Monte Carlo sampling technique. To ensure the tractability of the optimization problem, the large number of scenarios are reduced by using a backward-reduction algorithm based on Kantorovich Distance (KD) [27]. Then, for each scenario s, there is a travel time matrix denoted by $\mathbf{T}_s \in \mathbb{R}^{(|\mathcal{D}^R|+|\mathcal{F}^R|)\times(|\mathcal{D}^R|+|\mathcal{F}^R|)}$ and a repair time vector denoted by $\mathbf{T}_s^R \in \mathbb{R}^{|\mathcal{F}^R|}$. The (i,j)th element of $\mathbf{T}_s$ (i.e. $T_{ij,s}$) represents the travel time from site i to j and the i-th entry of $\mathbf{T}_s^R$ (i.e. $T_{i,s}^R$) indicates the repair time for the damaged component i.

The uncertainties in the third stage, i.e. uncertainties in electricity demand and maximum available PV power, are dynamically variant. Hence, it is difficult to identify their accurate PDFs and only limited information is available to characterize these uncertainties. Therefore, these uncertainties are represented by an uncertainty set $\mathcal{U}$ as formed by (1a)-(1f).

$$\mathcal{U} := \Big\{(\overline{p}_{i,t}^d, \overline{p}_{i,t}^{pv}) \Big|\ \overline{p}_{i,t}^d = p_{i,t}^{dn} + (z_{i,t}^{du} - z_{i,t}^{dl})\hat{p}_{i,t}^d, \tag{1a}$$

$$\overline{p}_{i,t,s}^{pv} = p_{i,t}^{pvn} + (z_{i,t}^{pvu} - z_{i,t}^{pvl})\hat{p}_{i,t}^{pv}, \tag{1b}$$

$$\sum_{i\in\mathcal{N}} \left(z_{i,t}^{du} + z_{i,t}^{dl}\right) \le \Gamma_N^d, \tag{1c}$$

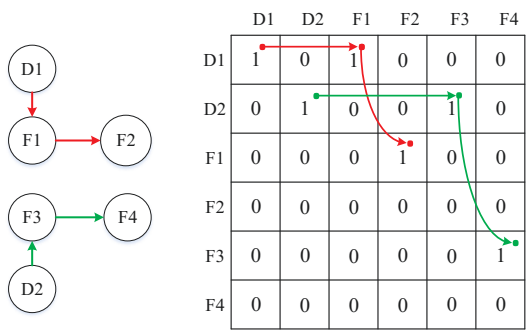

Fig. 2. An example of crew route decision and its corresponding route table

$$\sum_{t\in\mathcal{T}}\left(z^{du}_{i,t}+z^{dl}_{i,t}\right)\le\Gamma^{d}_{T}, \tag{1d}$$

$$\sum_{i\in\mathcal{N}^{pv}}\left(z^{pvu}_{i,t}+z^{pvl}_{i,t}\right)\le\Gamma^{pv}_{N}, \tag{1e}$$

$$\sum_{t\in\mathcal{T}}\left(z^{pvu}_{i,t}+z^{pvl}_{i,t}\right)\le\Gamma^{pv}_{T}\ \Big\} \tag{1f}$$

Constraints (1a) and (1b) show that for each time interval t and each node i, the actual requested electricity demand $\overline{p}^{d}_{i,t,s}$ and maximum available PV generation $\overline{p}^{pv}_{i,t,s}$ are within the ranges $(p^{dn}_{i,t}-\hat{p}^{d}_{i,t}, p^{dn}_{i,t}+\hat{p}^{d}_{i,t})$ and $(p^{pvn}_{i,t}-\hat{p}^{pv}_{i,t}, p^{pvn}_{i,t}+\hat{p}^{pv}_{i,t})$, respectively. Constraints (1c)-(1f) enforce the uncertainty budget to control the robustness of the model.

C. First Stage: Crew Dispatch

The route table is adopted to properly represent the crew routing option and to link it with the repair completion time of each damaged component. Essentially, the route table is a $(|\mathcal{D}^R|+|\mathcal{F}^R|)$-dimension square matrix (i.e. $\mathbf{x}^R$) composed of binary entries. Specifically, if the off-diagonal element x^R_{ij} equals to 1, it means a crew directly travels from site i to site j; if a diagonal element x^R_{ii} equals to 1, it indicates that site i is the starting point of a crew, i.e. site i is a depot site. Fig. 2 shows an example of the crew route decision and its corresponding route table representation. Base on these properties, the constraints associated with the crew route decision are summarized as (2)-(7), where (2) and (3) enforce that the routes of the crews can only be started from the depots; (4) ensures that the crews cannot travel from the damaged sites to the depot sites (unless all damages have been repaired); (5) implies that each edge on the routes cannot be visited more than once; (6) imposes a capacity limit on the number of crews departed from each depot site; (7) indicates that each damaged component is only visited by one crew and the number of crews departed from one site should not exceed the number of crews arrived. Note that the crew route decision is made prior to the realization of any uncertainty and hence is served as a "here-and-now" decision.

$$x^R_{ii}=1\quad\forall i\in\mathcal{D}^R \tag{2}$$

$$x^R_{ii}=0\quad\forall i\in\mathcal{F}^R \tag{3}$$

$$x^R_{ij}=0\quad\forall i\in\mathcal{F}^R, j\in\mathcal{D}^R \tag{4}$$

$$x^R_{ij}+x^R_{ji}\le 1\quad\forall i,j\in\mathcal{F}^R\cup\mathcal{D}^R \tag{5}$$

$$\sum_{j\in\mathcal{F}^R}x^R_{ij}\le N^R_i\quad\forall i\in\mathcal{D}^R \tag{6}$$

$$\sum_{j\in(\mathcal{F}^R\cup\mathcal{D}^R)\setminus i}x^R_{ij}\le\sum_{h\in(\mathcal{F}^R\cup\mathcal{D}^R)\setminus i}x^R_{hi}=1\quad\forall i\in\mathcal{F}^R \tag{7}$$

D. Second Stage: Switching Operation

To carry out the sequential switching operations, the repair completion times of damages need to be derived. To this end, the arrival time at each site will be calculated first based on the crew route option as well as the travel time and repair time corresponding to each damage using the big-M method. The relevant constraints are presented as (8)-(12) for each scenario s, where (8) specifies the current time as the departure time of each repair crew from the depot sites; (9) and (10) imply the relationship between the departure time from depot i and the arrival time at damaged component j. If the edge (i,j) is traversed by a crew, i.e. $x^R_{ij}=1$, then the arrival time at site j equals to the departure time from site i plus the travel time $T_{ij,s}$; otherwise, $T^A_{j,s}$ will not be constrained by these two constraints. Similarly, (11) and (12) show if a crew directly travels from the damaged site i to the damaged site j, the arrival time at site j equals to the arrival time at site i plus the repair time $T^R_{i,s}$ and the travel time $T_{ij,s}$.

$$T^A_{i,s}=t_0\quad\forall i\in\mathcal{D}^R \tag{8}$$

$$T^A_{j,s}\ge T^A_{i,s}+T_{ij,s}-(1-x^R_{ij})M\quad\forall i\in\mathcal{D}^R, j\in\mathcal{F}^R \tag{9}$$

$$T^A_{j,s}\le T^A_{i,s}+T_{ij,s}+(1-x^R_{ij})M\quad\forall i\in\mathcal{D}^R, j\in\mathcal{F}^R \tag{10}$$

$$T^A_{j,s}\ge T^A_{i,s}+T^R_{i,s}+T_{ij,s}-(1-x^R_{ij})M\quad\forall i,j\in\mathcal{F}^R \tag{11}$$

$$T^A_{j,s}\le T^A_{i,s}+T^R_{i,s}+T_{ij,s}+(1-x^R_{ij})M\quad\forall i,j\in\mathcal{F}^R \tag{12}$$

Constraints (13) and (14) translate the repair completion time $(T^A_{i,s}+T^R_{i,s})$ of each damaged component to the corresponding repair completion time interval $(\forall i\in\mathcal{F}^R, s\in\mathcal{S})$, where (13) ensures that for each damaged component only one indicator $e_{i,t,s}$ equals to 1 over the entire horizon; (14) determines the time interval within which the damage component i is repaired, where ϵ is a very small number.

$$\sum_{t\in\mathcal{T}}e_{i,t,s}=1 \tag{13}$$

$$T^A_{i,s}+T^R_{i,s}\le\sum_{t\in\mathcal{T}}t\times e_{i,t,s}\le T^A_{i,s}+T^R_{i,s}+1-\epsilon \tag{14}$$

Then, the constraints pertained to the line availability states and the switching operations can be formulated as (15)-(18) $(\forall t\in\mathcal{T}, s\in\mathcal{S})$. Constraint (15) shows that the damaged lines become immediately available once they are repaired. Here, $\mathcal{L}^d$ is the set of damaged lines and $n(j,k)$ maps the line index (j,k) to the damaged site index n. Furthermore, (16) illustrates that the non-damaged and non-switchable lines are closed all the time. Here, $\mathcal{L}^n$ is the set of non-switchable lines. Constraint (17) enforces faults' isolation by opening the upstream and downstream switches, where $\mathcal{W}^U_{jk}$ and $\mathcal{W}^D_{jk}$ are the sets of the upstream and downstream switches of line (j,k), respectively. Constraint (18) is to avoid loop formation,

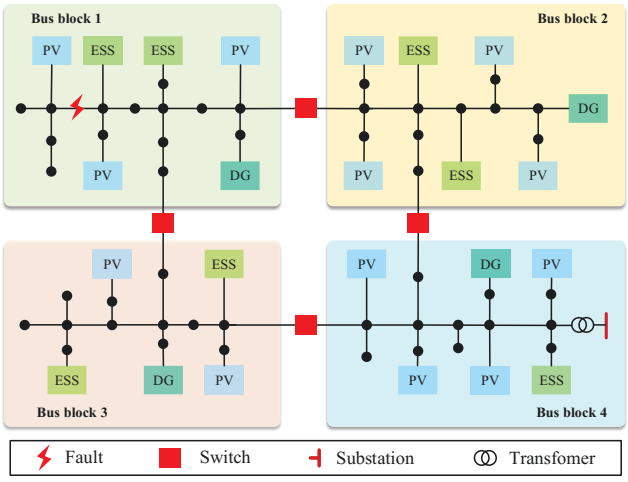

Fig. 3. An example of four bus blocks partitioned by switches

where $\mathcal{B}(l)$ is the set of lines in potential loop l and $\mathcal{O}$ is the set of potential loops.

$$u_{jk,t,s} = \sum_{\tau=1}^{t} e_{n(j,k),\tau,s} \qquad \forall (j,k) \in \mathcal{L}^d \tag{15}$$

$$u_{jk,t,s} = 1 \qquad \forall (j,k) \in \mathcal{L}^n \backslash \mathcal{L}^d, \tag{16}$$

$$u_{hi,t,s} \le u_{jk,t,s} \qquad \forall (j,k) \in \mathcal{L}^d, (h,i) \in \mathcal{W}_{jk}^U \cup \mathcal{W}_{jk}^D \tag{17}$$

$$\sum_{(j,k)\in\mathcal{B}_l} u_{jk,t,s} \le |\mathcal{B}_l| - 1 \qquad \forall l \in \mathcal{O} \tag{18}$$

Generally, the number of switches is much less than the number of lines in a DN. Thus, some buses can be grouped such that there is no switchable line in each group. Such group is referred to as a bus block. Adopting bus blocks could help reduce a large number of decision variables and constraints and thereby improve the computation efficiency substantially. A more intuitive illustration of the bus block is demonstrated in Fig. 3 where the switches partition the DN into four bus blocks and each bus block may have some DER installations. To indicate whether the bus block is energized or not after power outages, a binary variable $y_{k,t,s}$ is introduced. Note that a bus block cannot be energized before the clearance of its internal faults, as enforced by (19). Here, $\mathcal{L}_k$ is the set of lines within the bus block k.

$$y_{k,t,s} \le u_{ij,t,s} \qquad \forall (i,j) \in \mathcal{L}_k, t \in \mathcal{T}, s \in \mathcal{S} \tag{19}$$

Moreover, a bus block without black-start DERs can only be energized by external sources. To illustrate the energization process of the bus blocks, virtual power flow constraints (20)-(22) are introduced by treating each bus block as a virtual node ($\forall t \in \mathcal{T}, s \in \mathcal{S}$). Here, (20) represents the virtual power flow balance at each bus block k, where $\mathcal{G}_k$ is the set of DG units in block k and $\mathcal{L}^s$ is the set of switchable lines. The energization status $y_{k,t,s}$ is associated with virtual power load of block k. Here, (21) requires the outputs of the non-black-start units to be 0 and (22) imposes the capacity limits on the switchable lines.

$$\sum_{i\in\mathcal{G}_k} g_{i,t,s} + \sum_{(i,k)\in\mathcal{L}^s} f_{ik,t,s} = y_{k,t,s} + \sum_{(k,j)\in\mathcal{L}^s} f_{kj,t,s} \quad \forall k \in \mathcal{K} \tag{20}$$

$$g_{i,t,s} = 0 \quad \forall i \in \mathcal{G}^{nb} \tag{21}$$

$$-u_{ik,t,s} M \le f_{ik,t,s} \le u_{ik,t,s} M \quad \forall (i,k) \in \mathcal{L}^s \tag{22}$$

The charging/discharging states of energy storage systems (ESSs) are determined in the second stage so that the third stage only contains continuous variables. Let the binary variable $z_{i,t,s}^{ch}$ denote the charging command of ESS i for time interval t. The actual charging state $z_{i,t,s}^{es}$ needs to be modified by incorporating the energization state of its local bus block as (23)-(25) ($\forall t \in \mathcal{T}, s \in \mathcal{S}$). Here, $\mathcal{E}_k$ is the set of ESS units in the bus block k. (23)-(25) indicate only when the local bus block is energized, i.e. $y_{k,t,s} = 1$, and charging command is activated, i.e. $z_{i,t,s}^{ch} = 1$, the actual charging status will be 1.

$$z_{i,t,s}^{es} \le y_{k,t,s} \quad \forall i \in \mathcal{E}_k \tag{23}$$

$$z_{i,t,s}^{es} \le z_{i,t,s}^{ch} \quad \forall i \in \mathcal{E}_k \tag{24}$$

$$z_{i,t,s}^{es} \ge y_{k,t,s} + z_{i,t,s}^{ch} - 1 \quad \forall i \in \mathcal{E}_k \tag{25}$$

E. Third Stage: Optimal Scheduling of DERs

In the third stage, the line availability states and bus block energization states are known. Then, the optimal scheduling of DERs and demand curtailment will be determined to minimize the network operation cost plus the total curtailment charges. The objective function is presented as (26).

$$\min_{\mathbf{z}_s} \sum_{s\in\mathcal{S}} \Pr(s) \sum_{t\in\mathcal{T}} \Big(c_t^{grid} P_{01,t,s} + \sum_{i\in\mathcal{N}^{dg}} c_i^{dg} p_{i,t,s}^{dg} + \sum_{i\in\mathcal{N}} c_{i,t}^{d} (\overline{p}_{i,t,s}^{d} - p_{i,t,s}^{d}) \Big) \Delta t \tag{26}$$

The constraints of the third-stage problem contain power flow equations, line capacity limits, voltage limits, demand curtailment limits, and DER operation limits, as shown in (27a)-(27p).

$$\sum_{(i,j)\in\mathcal{L}} P_{ij,t,s} - \sum_{(k,i)\in\mathcal{L}} P_{ki,t,s} = p_{i,t,s}^{dg} + p_{i,t,s}^{pv} - p_{i,t,s}^{d} + p_{i,t,s}^{dch} - p_{i,t,s}^{ch} \quad \forall i \in \mathcal{N} \tag{27a}$$

$$\sum_{(i,j)\in\mathcal{L}} Q_{ij,t,s} - \sum_{(k,i)\in\mathcal{L}} Q_{ki,t,s} = q_{i,t,s}^{dg} + q_{i,t,s}^{pv} - q_{i,t,s}^{d} \quad \forall i \in \mathcal{N} \tag{27b}$$

$$v_{i,t,s} - v_{j,t,s} = 2(r_{ij} P_{ij,t,s} + x_{ij} Q_{ij,t,s}) \quad \forall (i,j) \in \mathcal{L} \tag{27c}$$

$$-u_{ij,t,s} \overline{P}_{ij} \le P_{ij,t,s} \le u_{ij,t,s} \overline{P}_{ij} \quad \forall (i,j) \in \mathcal{L} \tag{27d}$$

$$-u_{ij,t,s} \overline{Q}_{ij} \le Q_{ij,t,s} \le u_{ij,t,s} \overline{Q}_{ij} \quad \forall (i,j) \in \mathcal{L} \tag{27e}$$

$$\underline{V}_i^2 \le v_{i,t,s} \le \overline{V}_i^2 \quad \forall i \in \mathcal{N} \tag{27f}$$

$$0 \le p_{i,t,s}^{d} \le \overline{p}_{i,t,s}^{d} \quad \forall i \in \mathcal{N} \tag{27g}$$

$$q_{i,t,s}^{d} = \tan\beta \cdot p_{i,t,s}^{d} \quad \forall i \in \mathcal{N} \tag{27h}$$

$$y_{k(i),t,s} \underline{p}_i^{dg} \le p_{i,t,s}^{dg} \le y_{k(i),t,s} \overline{p}_i^{dg} \quad \forall i \in \mathcal{N}^{dg} \tag{27i}$$

$$y_{k(i),t,s} \underline{q}_i^{dg} \le q_{i,t,s}^{dg} \le y_{k(i),t,s} \overline{q}_i^{dg} \quad \forall i \in \mathcal{N}^{dg} \tag{27j}$$

$$0 \le p_{i,t,s}^{pv} \le y_{k(i),t,s} \overline{p}_{i,t,s}^{pv} \quad \forall i \in \mathcal{N}^{pv} \tag{27k}$$

$$y_{k(i),t,s}\underline{q}^{pv}_{i,t,s} \le q^{pv}_{i,t,s} \le y_{k(i),t,s}\overline{q}^{pv}_{i,t,s} \quad \forall i \in \mathcal{N}^{pv} \tag{27l}$$

$$0 \le p^{ch}_{i,t,s} \le z^{es}_{i,t,s}\overline{p}^{ch}_{i} \quad \forall i \in \mathcal{N}^{es} \tag{27m}$$

$$0 \le p^{dch}_{i,t,s} \le (y_{k(i),t,s} - z^{es}_{i,t,s})\overline{p}^{dch}_{i} \quad \forall i \in \mathcal{N}^{es} \tag{27n}$$

$$\text{SoC}_{i,t,s} = \text{SoC}_{i,t-1,s} + \Delta t(\eta^{ch}_i p^{ch}_{i,t,s} - \frac{p^{dch}_{i,t,s}}{\eta^{dch}_i}) \quad \forall i \in \mathcal{N}^{es} \tag{27o}$$

$$\underline{\text{SoC}}_i \le \text{SoC}_{i,t,s} \le \overline{\text{SoC}}_i \quad \forall i \in \mathcal{N}^{es} \tag{27p}$$

The linearized branch flow model is employed to represent the AC power flow in radial DNs [28]. (27a) and (27b) represent the active and reactive power balance constraints at each bus, respectively. (27c) shows the relationship between the squared nodal voltage magnitudes on adjacent buses. (27d) and (27e) show that the line flows cannot exceed their capacities considering the line availability states. (27f) imposes the limits on squared nodal voltage magnitudes. (27g) implies that the restored electricity demand cannot exceed the total electricity demand at each bus and (27h) relates the reactive demand to the active demand using a given power factor $\cos\beta$. (27i) and (27j) impose the upper and lower limits on the active and reactive power output of DG i, where $k(i)$ maps node index i to the corresponding bus block index k. (27k) ensures that the active power output of each PV should not exceed the maximum available PV power. Note that both DG and PV units are unable to generate power unless their local bus blocks are energized, i.e. $y_{k(i),t,s} = 1$. (27l) enforces the upper and lower limits on the reactive power of PV unit i, where $\overline{q}^{pv}_{i,t,s} = \sqrt{(S^{pv}_i)^2 - (\overline{p}^{pv}_{i,t,s})^2}$ and $\underline{q}^{pv}_{i,t,s} = -\overline{q}^{pv}_{i,t,s}$. (27m) and (27n) impose the limits on charging and discharging power of ESS unit i, respectively. The simultaneous charging and discharging situation is avoided. (27o) shows the variation of the state of charge (SOC) in ESS i and (27p) imposes the upper and lower limits on the SOC.

F. Proposed Multi-stage Co-Optimization Model

As discussed in subsection II-A, the proposed hybrid model for the distribution network restoration is formulated as a multi-stage co-optimization problem. In particular, the first stage is to determine the crew dispatch which is deterministic. The second stage is modeled as a stochastic programming and the third stage is formulated as a robust optimization problem. The proposed hybrid modeling based multi-stage problem is presented as (28a)-(28d).

$$\min_{\mathbf{x},\mathbf{y}_s} \max_{\mathbf{u}_s \in \mathcal{U}} \min_{\mathbf{z}_s} \sum_{s\in\mathcal{S}} \Pr(s) \sum_{t\in\mathcal{T}} \Big(c^{grid}_t P_{01,t,s} + \sum_{i\in\mathcal{N}^{dg}} c^{dg}_i p^{dg}_{i,t,s} + \sum_{i\in\mathcal{N}} c^{d}_{i,t}(\overline{p}^{d}_{i,t,s} - p^{d}_{i,t,s}) \Big) \Delta t \tag{28a}$$

$$\text{s.t. (2)-(7)} \tag{28b}$$

$$\text{(8)-(25)} \tag{28c}$$

$$\text{(27a)-(27p)} \tag{28d}$$

Note that the objective function has three layers. The inner layer is to search for an optimal third-stage solution to minimize the expected total cost concerning the uncertainty scenarios of travel and repair times. The mid-layer is to find the worst-case realizations of the electricity demand and PV generation by maximizing the optimal value of the inner layer problem. The outer layer is to search for the optimal crew route solution (i.e. $\mathbf{x}$) as well as the sequential switching actions (i.e. $\mathbf{y}_s$) for each scenario s. (28b), (28c) and (28d) collect the first-stage, second-stage and third-stage constraints, respectively.

III. Solution Methodology

The proposed hybrid multi-stage co-optimization model can be written compactly as (29a)-(29f).

$$\min_{\mathbf{x},\mathbf{y}_s} \sum_{s\in\mathcal{S}} \Pr(s) \Big[\max_{\mathbf{u}_s\in\mathcal{U}} \big(\mathbf{a}^\top \mathbf{u}_s + \min_{\mathbf{z}_s} \mathbf{b}^\top \mathbf{z}_s \big) \Big] \tag{29a}$$

$$\text{s.t. } \mathbf{A}\mathbf{x} \le \mathbf{c} \tag{29b}$$

$$\mathbf{B}\mathbf{x} + \mathbf{C}\mathbf{y}_s \le \mathbf{d}_s \qquad s \in \mathcal{S} \tag{29c}$$

$$\mathbf{D}\mathbf{z}_s \le \mathbf{f} \qquad : \boldsymbol{\lambda}_s \quad s \in \mathcal{S} \tag{29d}$$

$$\mathbf{E}\mathbf{z}_s + \mathbf{F}\mathbf{y}_s \le \mathbf{g} \qquad : \boldsymbol{\pi}_s \quad s \in \mathcal{S} \tag{29e}$$

$$\mathbf{G}\mathbf{z}_s + \mathbf{H}\mathbf{u}_s \le \mathbf{w} \qquad : \boldsymbol{\phi}_s \quad s \in \mathcal{S} \tag{29f}$$

where (29b) and (29c) summarize the first-stage and second-stage constraints, respectively; (29d)-(29f) summarize the third-stage constraints; $\boldsymbol{\lambda}_s, \boldsymbol{\pi}_s$ and $\boldsymbol{\phi}_s$ are corresponding dual variables. Note that the first-stage variables are only coupled with the second-stage variables and the third-stage variables are coupled with the second-stage variables as well as the uncertainties.

CCG method is employed to decompose the above problem into a master problem and a subproblem. The master problem is a relaxation of the original problem as shown by (30) and hence, provides a lower bound for the original problem.

$$\min_{\mathbf{x},\mathbf{y}_s,\mathbf{z}_{s,l}} \sum_{s\in\mathcal{S}} \Pr(s)\eta_s \tag{30a}$$

$$\text{s.t. (29b), (29c)} \tag{30b}$$

$$\eta_s \ge \mathbf{a}^\top \mathbf{u}^*_{s,l} + \mathbf{b}^\top \mathbf{z}_{s,l} \quad s \in \mathcal{S}, l = 1, ..., k \tag{30c}$$

$$\mathbf{D}\mathbf{z}_{s,l} \le \mathbf{f} \quad s \in \mathcal{S}, l = 1, ..., k \tag{30d}$$

$$\mathbf{E}\mathbf{z}_{s,l} + \mathbf{F}\mathbf{y}_s \le \mathbf{g} \quad s \in \mathcal{S}, l = 1, ..., k \tag{30e}$$

$$\mathbf{G}\mathbf{z}_{s,l} + \mathbf{H}\mathbf{u}^*_{s,l} \le \mathbf{w} \quad s \in \mathcal{S}, l = 1, ..., k \tag{30f}$$

Here, (30c)-(30f) represent the iteratively added CCG cuts, and $\mathbf{u}^*_{s,l}$ is the worst-case realization of the third-stage uncertain variables obtained by solving the subproblem at l-th iteration.

The subproblem is essentially the third-stage problem with the given first two-stage variables and thus provides an upper bound for the original problem. Note that the third-stage subproblem can be further decomposed into $|\mathcal{S}|$ subproblems with each only associated with one scenario. Then, given the variable $\mathbf{y}_s$, the third-stage subproblem for scenario s can be written as (31).

$$\max_{\mathbf{u}_s\in\mathcal{U}} \big(\mathbf{a}^\top \mathbf{u}_s + \min_{\mathbf{z}_s} \mathbf{b}^\top \mathbf{z}_s \big) \tag{31a}$$

$$\text{s.t. (29d)-(29f)} \tag{31b}$$

The above "max-min" problem is equivalently converted into a single level maximization problem (32) by replacing the inner level with its dual.

$$\max_{\mathbf{u}_s,\boldsymbol{\lambda}_s,\boldsymbol{\pi}_s,\boldsymbol{\phi}_s} \mathbf{a}^\top \mathbf{u}_s - \mathbf{f}^\top \boldsymbol{\lambda}_s + \mathbf{y}_s^\top \mathbf{F}^\top \boldsymbol{\pi}_s - \mathbf{g}^\top \boldsymbol{\pi}_s + \mathbf{u}_s^\top \mathbf{H}^\top \boldsymbol{\phi}_s$$

$$-\mathbf{w}^{\top}\boldsymbol{\phi}_s \tag{32a}$$

$$\text{s.t. } \mathbf{D}^{\top}\boldsymbol{\lambda}_s + \mathbf{E}^{\top}\boldsymbol{\pi}_s + \mathbf{G}^{\top}\boldsymbol{\phi}_s = -\mathbf{b} \tag{32b}$$

$$\boldsymbol{\lambda}_s \geq 0, \quad \boldsymbol{\pi}_s \geq 0, \quad \boldsymbol{\phi}_s \geq 0 \tag{32c}$$

$$\mathbf{u}_s \in \mathcal{U} \tag{32d}$$

Since $\mathbf{u}_s^{\top}\mathbf{H}^{\top}\boldsymbol{\phi}_s$ in (32a) is a bilinear term, the problem (32) is a bilinear programming problem with linear constraints. Alternating direction method can be used to solve it [29].

To enhance the computation efficiency in practical applications, parallel computing can be invoked for solving the third-stage subproblem thanks to its decomposable structure. In fact, the master problem can also be decomposed into $|\mathcal{S}|$ subproblems using PH method [30] and each subproblem is only associated with one specific scenario.

Fig. 4 shows the flowchart of the proposed algorithm for solving the hybrid multi-stage co-optimization model (29) based on the CCG and PH methods. The first step is to initialize the lower/upper bounds and the iteration index. There are two loops in the algorithm. The inner loop starts with step 2 and ends with step 8, which is for solving the master problem (30) using the PH method. The outer loop, consisting of step 2 to step 13, is to solve the problem (29) using the CCG method. Specifically, step 4 is to update the first two-stage variables for each scenario s. Then at the 5th step, the weighted average of the first stage variables is calculated followed by the update of the auxiliary variable Ψ_s at step 6. When the condition at step 8 is satisfied, the solution $\mathbf{x}_{s,m}$ converges to $\overline{\mathbf{x}}_m$ and the solution to the master problem is obtained. Then, the lower bound of the problem (29) is updated and the procedure for solving the subproblem (32) begins at step 10. Next, the new CCG cuts are generated and added to the master problem. Finally, when the condition at step 13 is met, the solution is converged and the algorithm terminates.

IV. Numerical Results

The proposed hybrid model for the outage management scheme is tested on the modified IEEE 37-bus distribution test feeder. The detailed information about the test feeder including the electricity demand data and line parameters can be found in [31]. The nominal voltage is 4.8 kV and the per-unit value is used in the case studies. Fig. 5 shows the network topology where the locations of DERs are also indicated. Two DGs with black-start capability are installed to facilitate service restoration after the power outages. The distribution system also includes eight PV units, two of them coupled with ESS. The parameters related to the DERs and their marginal operation cost are listed in Table I. Without loss of generality, it is assumed that four lines are damaged as shown in Fig. 5. Three case studies are carried out to validate the effectiveness of the proposed scheme. In the first study, the computation performance as well as the restoration process are discussed by analyzing the simulation results. In the second one, the performance of the proposed scheme is compared with a recently proposed benchmark scheme [19]. In the last study, a sensitivity analysis is conducted to investigate the effect of the number of depots on restoration performance. In the first two studies, two crews are dispatched from Depots 1 and 2 to repair the damages, respectively.

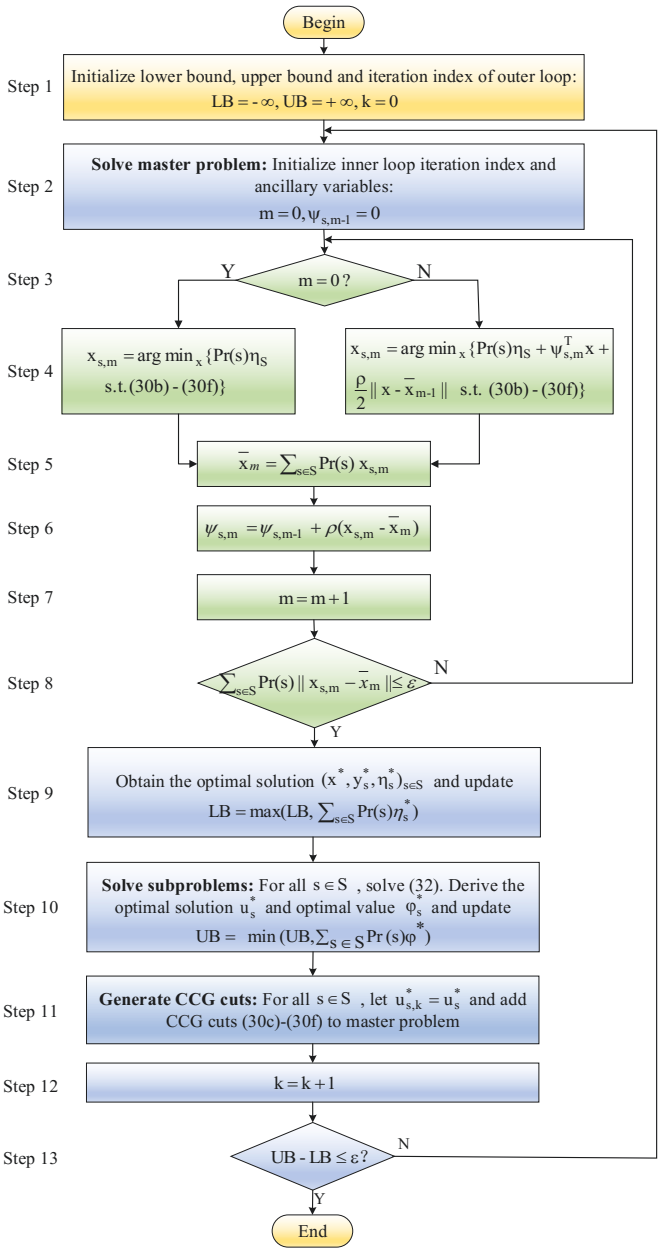

Fig. 4. Flowchart of CCG and PH based algorithm for solving the hybrid modeling based multi-stage co-optimization problem (29)

TABLE I
Values of Parameters Related to DERs and Operation Cost

Paramt	Value	Paramt	Value	Paramt	Value
$\overline{p}_i^{dg}$	200 kW	$\underline{p}_i^{dg}$	0 kW	c_i^{dg}	\$0.1/kWh
$\overline{q}_i^{dg}$	100 kVar	$\underline{q}_i^{dg}$	0 kVar	c_t^{grid}	\$0.06/kWh
$\overline{p}_i^{ch}$	50 kW	$\overline{p}_i^{dch}$	50 kW	$c_{i,t}^{d}$	\$50/kWh
$\overline{\text{SoC}}_i$	300kWh	$\underline{\text{SoC}}_i$	30kWh	S_i^{pv}	200 kVA
η_i^{ch}	95%	η_i^{dch}	95%	$\underline{V}_i/\overline{V}_i$	0.95/1.05 p.u.

The mean values of the travel times on the path between

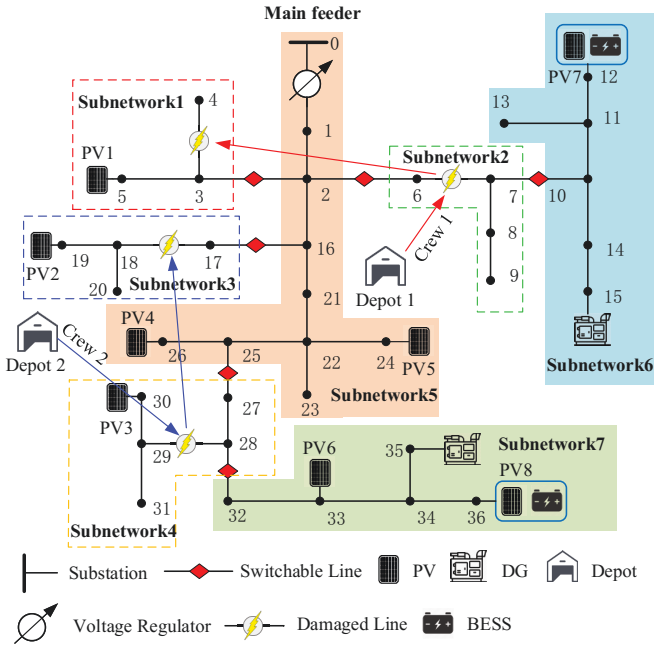

Fig. 5. IEEE 37-bus distribution system after 4 lines are damaged

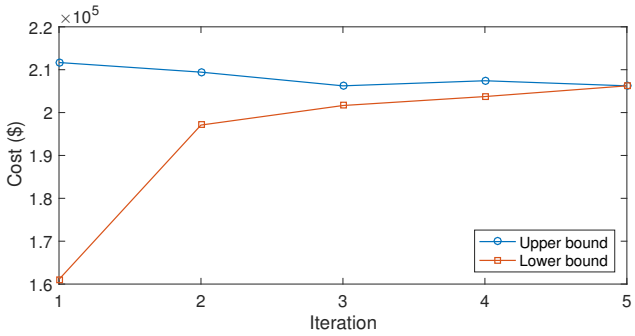

Fig. 6. Convergence of upper and lower bounds using the proposed algorithm

any pair of sites are obtained by dividing the distance by the average traveling speed. To account for the uncertain traffic condition, the standard deviation of the travel time is assumed to be 5% of the mean. It is assumed that the repair time follows the lognormal distribution with parameters $\mu = 0.9163$ and $\sigma = 0.06$ [26]. Then, 100 scenarios of travel and repair times are generated and reduced to 5 representative ones using the backward-reduction algorithm [27]. The solar PV generation data for a typical day, obtained from [32], is used as nominal values ($p_{i,t}^{pvn}$). The deviations of the upper/lower bounds ($\hat{p}_{i,t}^{pv}$) are selected as 30% of the nominal values. Similarly, the deviations of the upper/lower bounds of the electricity demand ($\hat{p}_{i,t}^{d}$) are considered to be 20% of the nominal values ($p_{i,t}^{dn}$). The duration of the formulated problem and the time step are selected as 8 hours and 1 hour, respectively. Finally, the simulation is implemented using MATLAB on a personal computer with an Intel Core i7 of 2.5GHz and 16GB memory.

TABLE II
REPAIR COMPLETION TIMES OF DAMAGES AND SWITCH CLOSED TIMES

Faults	Repair completion time (hour)	Upper stream switch	Closing time (hour)	Down stream switch	Closing time (hour)
line 3-4	5.52	line 2-3	6	None	-
line 6-7	2.65	line 2-6	3	line 7-10	3
line 17-18	5.42	line 16-17	6	None	-
line 28-29	2.58	line 25-27	3	line 28-32	3

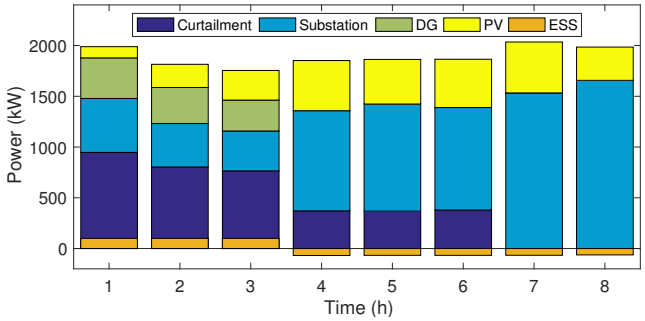

Fig. 7. Demand curtailment and active power delivered by DG, PV, ESS and Substation

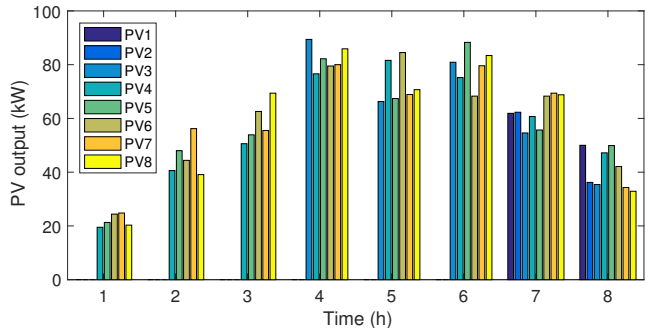

Fig. 8. Active power outputs of each PV unit at each time interval

A. Simulation Validation

Fig. 6 depicts the convergence of upper and lower bounds using the proposed algorithm. It is shown that the results converge with only 5 iterations and the total computation time is 98.99 seconds which well fits the real-time application.

The crew dispatch results are illustrated in Fig. 5. As can be seen, Crew 1 is first dispatched from Depot 1 to the damaged line 6-7 and then line 3-4; Crew 2 is first mobilized from Depot 2 to the damaged line 28-29 and then line 17-18. Fig. 5 also shows that after outages, the network is partitioned into 7 parts and all switches are opened to isolate the faults. Subnetworks 1-4 are faulted areas and are de-energized immediately. Only one part (i.e. Subnetwork 5) is still connected to the main grid and operated normally. The other two parts (i.e. Subnetwork 6 and Subnetwork 7) are operated in the islanding mode and become isolated microgrids with the support of internal black-start DGs. Note that the crew dispatch decisions are obtained prior to the realization of the uncertainties. Thus, to evaluate the restoration performance, a scenario of random variables are generated to account for the realization of the uncertainties.

TABLE III
CREW ROUTING SOLUTIONS USING TWO DIFFERENT APPROACHES

Approaches	Route
HYB	Crew1: DP1 → line 6-7 → line 3-4 Crew2: DP2 → line 28-29 → line 17-18
SMDSR	Crew1: DP1 → line 17-18 → line 28-29 Crew2: DP2 → line 3-4 → line 6-7

TABLE IV
PERFORMANCE COMPARISON OF STATISTICAL DATA OF HYB AND SMDSR USING 300 RANDOMLY GENERATED SCENARIOS

Approaches	Curtailed demand (kWh)			Reduction in highest value
	Mean	std	Highest value	
HYB	3734.1	96.9	4072.3	3.3%
SMDSR	3735.8	162.9	4208.1	0

The repair completion times of the damaged lines and the closing times of switches, listed in Table II, are derived based on the crew dispatch solution as well as the realized travel and repair times. It is shown that after the restoration of damaged line 6-7, the upper-stream switch on line 2-6 and the down-stream switch on line 7-10 are closed subsequently. Consequently, Subnetwork 5, Subnetwork 2, and Subnetwork 6 are interconnected and all demands within the interconnected areas are served by the main feeder and DERs. Likewise, switches on line 25-27 and line 28-32 are closed following the restoration of damaged line 28-29. As a result, Subnetwork 5, Subnetwork 4, and Subnetwork 7 are interconnected. The last two restored areas are Subnetworks 1 and 3. The switch on line 16-17 is closed after the repair completion of damaged line 17-18 and the switch on line 2-3 is closed following the restoration of damaged line 3-4.

Fig. 7 depicts the total demand curtailment as well as the power supplied by the DERs and the substation at each time interval. It can be seen that the demand curtailment is reduced by half at the 4th hour as two damaged lines are repaired and eventually all loads are picked up at the 7th hour when the restoration is completed. It is also observed that after the outage, DGs are started to restore a large portion of loads within their local subnetworks and shut down when the local subnetworks are interconnected with the substation as the energy price of the main grid is lower than the marginal costs of DGs. Consequently, more and more power is supplied by the substation as more areas are restored and interconnected. ESSs also supply power to loads when the local generation is insufficient (1st-3rd hour) and replenish the stored energy when their local areas are connected to the areas supplied by the substation (4th-8th hour). Fig. 8 shows the outputs of PV units. As it is shown, PV4-PV8 are always available as their local subnetworks are energized at the beginning of the restoration. PV1-PV3 provide power after their local subnetworks are re-energized by the external sources.

B. Performance Comparisons

In this subsection, the performance of the proposed hybrid model for outage management, denoted as HYB, is compared

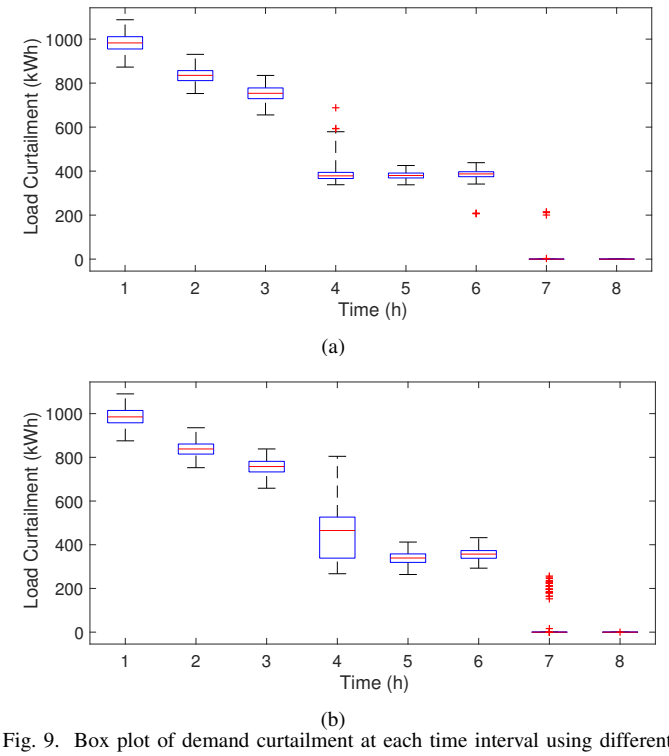

Fig. 9. Box plot of demand curtailment at each time interval using different schemes (a) HYB (b) SMDSR

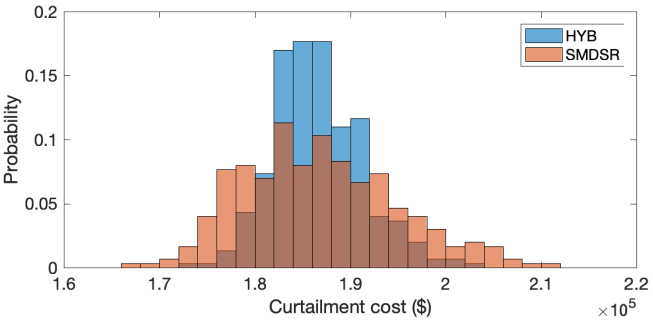

Fig. 10. Distribution of curtailment cost using HYB and SMDSR with 300 scenarios

with the performance of a benchmark scheme, denoted as SMDSR [19]. SMDSR is a recently proposed synthetic model of crew dispatch and distribution system restoration, which is formulated as a mixed-integer linear programming (MILP) model. Nevertheless, it does not take multiple sources of uncertainties into account during the restoration process. Thus, the mean values of travel/repair times and the nominal values of electricity demand/PV outputs are used in the SMDSR.

Table III demonstrates the crew routing solutions that are completely different using two different approaches. To conduct a comprehensive comparison, 300 scenarios of the random variables, are generated and the statistical outcomes of two approaches are summarized in Table IV. It is shown that the means of the curtailed demand are very close using these two approaches. However, the standard deviation (std) under HYB is 40.5% less than that using SMDSR. Furthermore, the highest demand curtailment is reduced by 3.3% when HYB

TABLE V
THE INFLUENCE OF THE NUMBER OF DEPOTS ON THE REPAIR COMPLETION TIME AND CURTAILED DEMAND

Cases	Repair completion time (hour)				Curtailed load (kWh)
	line 3-4	line 6-7	line 17-18	line 28-29	
1 depot	11.24	2.71	8.37	5.57	6336.5
2 depots	5.52	2.65	5.42	2.58	3635.5

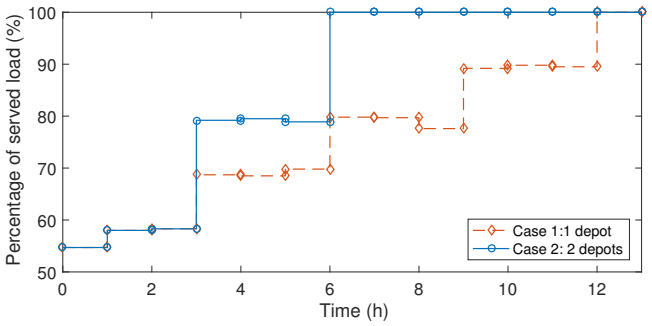

Fig. 11. Percentage of restored demand at each time interval with different number of depots

is applied, which implies that HYB is more robust than the SMDSR. It is worth mentioning that although the relative reduction in the highest demand curtailment may not seem significant, it could still reduce the curtailment costs considerably as the demand curtailment penalties are high. Fig. 9 shows the box plot of the demand curtailment at each time interval using the two schemes. The lower and upper bounds of the blue box represent the 25% and 75% quantiles, respectively. The dots denoted by the red cross symbol are outliers that have abnormal distances from other values. As shown in the figure, at 4th hour, the height of the box under HYB is much shorter than that under SMDSR. At 7th hour the number of outliers under HYB is much less than that under SMDSR, which further corroborates that the variance of the outcomes generated by HYB is lower than that procured using the SMDSR. Fig. 10 demonstrates the distributions of the demand curtailment cost using the two approaches. It can be observed from this figure that the curtailment costs under HYB are more concentrated compared to those using the SMDSR. Moreover, the highest curtailment cost using SMDSR is much higher than that using HYB. Therefore, our proposed scheme outperforms the benchmark scheme SMDSR in terms of hedging against the risk of high demand curtailment and reducing the variance of the restoration outcomes.

C. Sensitivity Analysis on the Number of Depots

In this subsection, a sensitivity analysis on the number of depots is conducted. Two cases are considered, i.e. Case 1 with only one depot and Case 2 with two depots. In addition, it is assumed that each depot has only one repair crew. Table V lists the repair completion time of each damaged line and the total curtailed demand in two cases, respectively. It can be seen that the total restoration time and total curtailed demand are almost doubled when the number of depots declines from 2 to 1. Fig.

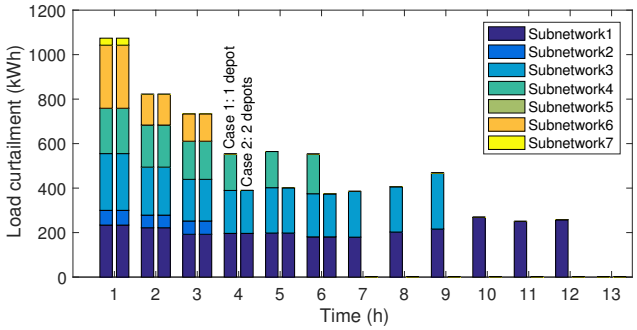

Fig. 12. Demand curtailment in different subnetworks with one depot site and two depots sits

11 depicts the percentage profiles of the restored demands. As shown in this figure, all loads are picked up by the 7th hour when 2 depots are available, while the restoration takes 12 hours to complete with only 1 depot. Fig. 12 shows the demand curtailment in each subnetwork at each time interval for Cases 1 and 2, respectively. We can observe from the figure that at the first three hours when no damage has been repaired, two cases have the same demand curtailment. At the 4th hour, two damaged lines are repaired in Case 2 and thus only two faulted areas (i.e. Subnetworks 1 and 3) suffer from demand curtailment, while in Case 1 only line 6-7 is repaired, and thus there are still three areas (i.e. Subnetworks 1, 3 and 4) that suffer from demand curtailment. At the 7th hour, all loads are restored in Case 2, while in Case 1 the demand curtailment exists in subnetwork 1 until the 13th hour. Thus, it can be concluded that the number of depots has a substantial influence on the restoration performance.

V. CONCLUSIONS

To expedite service restoration, a novel co-optimization based outage management scheme is proposed in this paper that captures the interdependence between crew dispatch and DSR. Since the decisions in outage management are implemented sequentially, the co-optimization of crew dispatch and DSR is formulated as a multi-stage problem. Specifically, the first stage is to search for the optimal crew route solution, while in the second and third stages the network reconfiguration and microgrid dispatch are determined, respectively. Furthermore, unlike most exiting works, multiple sources of uncertainties are taken into consideration. A novel hybrid modeling technique is developed to handle these uncertainties by modeling the second stage as a SP problem and the third stage as a RO problem. To efficiently solve the problem, an advanced solution method is developed based on CCG and PH approaches. Case studies on modified IEEE 37-bus DS show the computation time is quite short (< 100 seconds) and also demonstrate that the number of depots has a significant influence on the restoration outcome. Moreover, compared with a benchmark approach, the highest demand curtailment is reduced by 3.3% and the variance of restoration outcome is lowered by 40.5% using our proposed scheme.

REFERENCES

[1] R. J. Campbell and S. Lowry, "Weather-related power outages and electric system resiliency." Congressional Research Service, Library of Congress Washington, DC, 2012.

[2] "Hurricanes Nate, Maria, Irma, and Harvey Situation Reports," U.S. Department of Energy [online]. Available: https://www.energy.gov/ceser/downloads/hurricanes-nate-maria-irma-and-harvey-situation-reports.

[3] Y. Wang, C. Chen, J. Wang, and R. Baldick, "Research on resilience of power systems under natural disasters–a review," *IEEE Transactions on Power Systems*, vol. 31, no. 2, pp. 1604–1613, 2016.

[4] Y. Wang, Y. Xu, J. Li, J. He, and X. Wang, "On the radiality constraints for distribution system restoration and reconfiguration problems," *IEEE Trans. on Power Syst.*, vol. 35, no. 4, pp. 3294–3296, 2020.

[5] A. Gonzalez, F. M. Echavarren, L. Rouco, and T. Gomez, "A sensitivities computation method for reconfiguration of radial networks," *IEEE Trans. on Power Syst.*, vol. 27, no. 3, pp. 1294–1301, 2012.

[6] P. L. Cavalcante, J. C. López, J. F. Franco, M. J. Rider, A. V. Garcia, M. R. Malveira, L. L. Martins, and L. C. M. Direito, "Centralized self-healing scheme for electrical distribution systems," *IEEE Transactions on Smart Grid*, vol. 7, no. 1, pp. 145–155, 2016.

[7] W. Li, Y. Li, C. Chen, Y. Tan, Y. Cao, M. Zhang, Y. Peng, and S. Chen, "A full decentralized multi-agent service restoration for distribution network with dgs," *IEEE Transactions on Smart Grid*, vol. 11, no. 2, pp. 1100–1111, 2020.

[8] S. Lei, C. Chen, Y. Song, and Y. Hou, "Radiality constraints for resilient reconfiguration of distribution systems: Formulation and application to microgrid formation," *IEEE Transactions on Smart Grid*, vol. 11, no. 5, pp. 3944–3956, 2020.

[9] J. Li, C. Zhang, Z. Xu, J. Wang, J. Zhao, and Y.-J. A. Zhang, "Distributed transactive energy trading framework in distribution networks," *IEEE Transactions on Power Systems*, vol. 33, no. 6, pp. 7215–7227, 2018.

[10] P. Akaber, B. Moussa, M. Debbabi, and C. Assi, "Automated post-failure service restoration in smart grid through network reconfiguration in the presence of energy storage systems," *IEEE Systems Journal*, vol. 13, no. 3, pp. 3358–3367, 2019.

[11] T. Khalili, A. Bidram, and M. J. Reno, "Impact study of demand response program on the resilience of dynamic clustered distribution systems," *IET Generation, Transmission & Distribution*, vol. 14, no. 22, pp. 5230–5238, 2020.

[12] H. Sekhavatmanesh and R. Cherkaoui, "A multi-step reconfiguration model for active distribution network restoration integrating DG start-up sequences," *IEEE Transactions on Sustainable Energy*, vol. 11, no. 4, pp. 2879–2888, 2020.

[13] Z. Wang, B. Chen, J. Wang, and C. Chen, "Networked microgrids for self-healing power systems," *IEEE Transactions on smart grid*, vol. 7, no. 1, pp. 310–319, 2016.

[14] C. Chen, J. Wang, F. Qiu, and D. Zhao, "Resilient distribution system by microgrids formation after natural disasters," *IEEE Transactions on smart grid*, vol. 7, no. 2, pp. 958–966, 2016.

[15] A. Arif, Z. Wang, C. Chen, and J. Wang, "Repair and resource scheduling in unbalanced distribution systems using neighborhood search," *IEEE Transactions on Smart Grid*, vol. 11, no. 1, pp. 673–685, 2020.

[16] A. Arab, A. Khodaei, Z. Han, and S. K. Khator, "Proactive recovery of electric power assets for resiliency enhancement," *IEEE Access*, vol. 3, pp. 99–109, 2015.

[17] Y. Tan, F. Qiu, A. K. Das, D. S. Kirschen, P. Arabshahi, and J. Wang, "Scheduling post-disaster repairs in electricity distribution networks," *IEEE Trans. on Power Syst.*, vol. 34, no. 4, pp. 2611–2621, 2019.

[18] Y. Lin, B. Chen, J. Wang, and Z. Bie, "A combined repair crew dispatch problem for resilient electric and natural gas system considering reconfiguration and DG islanding," *IEEE Trans on Power Syst.*, vol. 34, no. 4, pp. 2755–2767, 2019.

[19] B. Chen, Z. Ye, C. Chen, J. Wang, T. Ding, and Z. Bie, "Toward a synthetic model for distribution system restoration and crew dispatch," *IEEE Transactions on Power Systems*, vol. 34, no. 3, pp. 2228–2239, 2019.

[20] B. Chen, Z. Ye, C. Chen, and J. Wang, "Toward a MILP modeling framework for distribution system restoration," *IEEE Transactions on Power Systems*, vol. 34, no. 3, pp. 1749–1760, 2019.

[21] S. Lei, C. Chen, Y. Li, and Y. Hou, "Resilient disaster recovery logistics of distribution systems: Co-optimize service restoration with repair crew and mobile power source dispatch," *IEEE Transactions on Smart Grid*, vol. 10, no. 6, pp. 6187–6202, 2019.

[22] S. Riahinia, A. Abbaspour, M. Moeini-Aghtaie, and S. Khalili, "Load service restoration in active distribution network based on stochastic approach," *IET Generation, Transmission & Distribution*, vol. 12, no. 12, pp. 3028–3036, 2018.

[23] X. Chen, W. Wu, and B. Zhang, "Robust restoration method for active distribution networks," *IEEE Transactions on Power Systems*, vol. 31, no. 5, pp. 4005–4015, 2016.

[24] J. R. Birge and F. Louveaux, *Introduction to stochastic programming*. Springer Science & Business Media, 2011.

[25] B. Chen, C. Chen, J. Wang, and K. L. Butler-Purry, "Sequential service restoration for unbalanced distribution systems and microgrids," *IEEE Transactions on Power Systems*, vol. 33, no. 2, pp. 1507–1520, 2018.

[26] C. J. Zapata, S. C. Silva, and O. L. Burbano, "Repair models of power distribution components," in *2008 IEEE/PES Transmission and Distribution Conference and Exposition: Latin America*, 2008, pp. 1–6.

[27] N. Growe-Kuska, H. Heitsch, and W. Romisch, "Scenario reduction and scenario tree construction for power management problems," in *2003 IEEE Bologna Power Tech Conference Proceedings*, 2003, pp. 7–15.

[28] M. Farivar and S. H. Low, "Branch flow model: Relaxations and convexification–part I," *IEEE Trans. on Power Syst.*, vol. 28, no. 3, pp. 2554–2564, 2013.

[29] A. Lorca and X. A. Sun, "Adaptive robust optimization with dynamic uncertainty sets for multi-period economic dispatch under significant wind," *IEEE Transactions on Power Systems*, vol. 30, no. 4, pp. 1702–1713, 2015.

[30] A. Arif, S. Ma, Z. Wang, J. Wang, S. M. Ryan, and C. Chen, "Optimizing service restoration in distribution systems with uncertain repair time and demand," *IEEE Transactions on Power Systems*, vol. 33, no. 6, pp. 6828–6838, 2018.

[31] W. H. Kersting, "Radial distribution test feeders," *IEEE Transactions on Power Systems*, vol. 6, no. 3, pp. 975–985, 1991.

[32] "Cooperative networks for renewable resource measurements solar energy resource data," National Renewable Energy Lab. (NREL) [online]. Available: https://www.nrel.gov/grid/solar-resource/confrrm.html.

Jiayong Li (Member, IEEE) received the B.Eng. degree from Zhejiang University, Hangzhou, China, in 2014, and the Ph.D. degree from The Hong Kong Polytechnic University, Hong Kong, in 2018. He is current an Assistant Professor with the the College of Electrical and Information Engineering of Hunan University. In 2019, he was with the Department of Electrical and Computer Engineering, Southern Methodist University as a Post Doctoral Fellow. He was also a Postdoctoral Research Fellow with The Hong Kong Polytechnic University and a Visiting Scholar with Argonne National Laboratory, Argonne, IL, USA. His research interests include distribution system planning and operation, power economics, demand-side energy management, and distributed control.

Mohammad E. Khodayar (Senior Member, IEEE) received the B.Sc. degree in electrical engineering from the Amirkabir University of Technology, Tehran, Iran, the M.S. degree in electrical engineering from the Sharif University of Technology, Tehran, and the Ph.D. degree in electrical engineering from the Illinois Institute of Technology, Chicago, IL, USA, in 2012. He was a Senior Research Associate with the Robert W. Galvin Center for Electricity Innovation, Illinois Institute of Technology. He is currently an Associate Professor with the Department of Electrical and Computer Engineering, Southern Methodist University, Dallas, TX, USA. His research interests include power system operation and planning. He is an Associate Editor of the IEEE Transactions on Sustainable Energy and the IEEE Transactions on Vehicular Technology.

Mohammad Ramin Feizi (Student Member, IEEE) received the B.Sc. degree in electrical engineering from Sahand University of Technology, Tabriz, Iran, in 2012 and the M.Sc. degree in electrical engineering from University of Kurdistan, Iran, in 2014. He is currently pursuing his Ph.D. degree in the department of Electrical and Computer Engineering at Southern Methodist University, Dallas, TX, USA. His research interests include optimization and power system operation and control.